Bi-directional modulation of contact thermal resistance between boron nitride nanotubes from a

polymer interlayer

Zhiliang Pan, ¹ Yi Tao, ² Yang Zhao, ¹ Matthew L. Fitzgerald, ¹ James McBride, ³ Lei Zhu, ⁴ and Deyu Li^{1,*}

¹Department of Mechanical Engineering, Vanderbilt University, Nashville, TN, 37235, USA

²School of Mechanical Engineering and Jiangsu Key Laboratory for Design and Manufacture of Micro-

Nano Biomedical Instruments, Southeast University, Nanjing, 210096, P. R. China.

³Department of Chemistry, The Vanderbilt Institute of Nanoscale Science and Engineering, Vanderbilt University, Nashville, TN 37235, USA

⁴Department of Macromolecular Science and Engineering, Case Western Reserve University, Cleveland, OH, 44106, USA

*: Author to whom correspondence should be addressed

E-mails: deyu.li@vanderbilt.edu

conductivity BNNT-polymer composites.

ABSTRACT: Enhancing the thermal conductivity of polymer composites could improve their performance in applications requiring fast heat dissipation. While significant progress has been made, a long-standing issue is the contact thermal resistance between the nanofillers, which could play a critical role in the composite thermal properties. Through systematic studies of contact thermal resistance between individual boron nitride nanotubes (BNNTs) of different diameters, with and without a poly(vinyl pyrrolidone) (PVP) interlayer, we show that the contact thermal resistance between bare BNNTs is largely determined by phonon reflection at the contact region. Interestingly, it is found that a PVP interlayer can either enhance or reduce the contact thermal resistance, as a result of converting the ballistic phonon dominated transport into diffusion through the PVP layer. These results disclose a previously unrecognized physical picture of thermal transport at the contact between BNNTs, which provides insights into the design of high thermal

KEYWORDS: Phonon transport, polymer composites, boron nitride nanotubes, thermal conductivity, thermal conductivity enhancement

1

Thermally conductive polymer composites are of current interest for various applications that require rapid heat dissipation.¹⁻³ Various filler materials, including carbon nanotubes (CNTs),⁴⁻⁶ ceramic particles,⁷⁻⁹ and metal nanowires¹⁰⁻¹³ have been tested for enhancing composite thermal conductivity. For applications as thermal interface materials in electronic/optoelectronic devices and as structural materials mounted with high power devices, it is highly desirable to have thermally conductive yet electrically insulating composites.¹⁴ Towards this goal, boron nitride nanotubes and nanosheets have been identified as promising filler materials to enhance the thermal conductivity of polymer composites without jeopardizing their electrical insulation properties.¹⁴⁻¹⁶ While significant progress has been made, issues related to the contact thermal resistance between these nanofillers, remain poorly understood.

Given the experimental challenge of directly measuring contact thermal resistance between nanostructures, traditionally its values have been inferred from the measured thermal conductivity of bulk composites using various effective media models.³ The values often vary drastically from each other in different studies and don't match well with expectations.^{3,17,18} Meanwhile, limited efforts on directly measuring contact thermal resistance between nanofillers have disclosed unusual observations, such as the diameter dependent contact thermal conductance per unit area between multi-walled CNTs (MWCNTs),¹⁹ which is regarded as size independent. In addition, one interesting question is the effect of a polymer interlayer on the contact thermal resistance as it often presents at the contact between nanofillers. Through systematic studies of the thermal resistance of the contacts between individual BNNTs with and without a PVP interlayer, here we report on the unexpected bi-directional modulation of the contact thermal resistance by a PVP interlayer.

To perform the experiment, BNNT suspension obtained *via* sonication of BNNT powder (NanoIntegris Technologies) was first drop-casted onto a piece of polydimethylsiloxane (PDMS).

Using a sharp probe mounted on a micromanipulator, an individual BNNT was broken into two segments, which were then transferred to the measurement device to form a contact sample for thermal measurement,²⁰⁻²² as shown in the scanning electron microscopy (SEM) image in Fig. 1a. Afterwards, one segment was realigned between the heat source and heat sink (Fig. 1b) for measuring the resistance of the single continuous tube. Comparison of these two measurement results allows for extraction of the thermal resistance of point contacts between bare BNNTs.

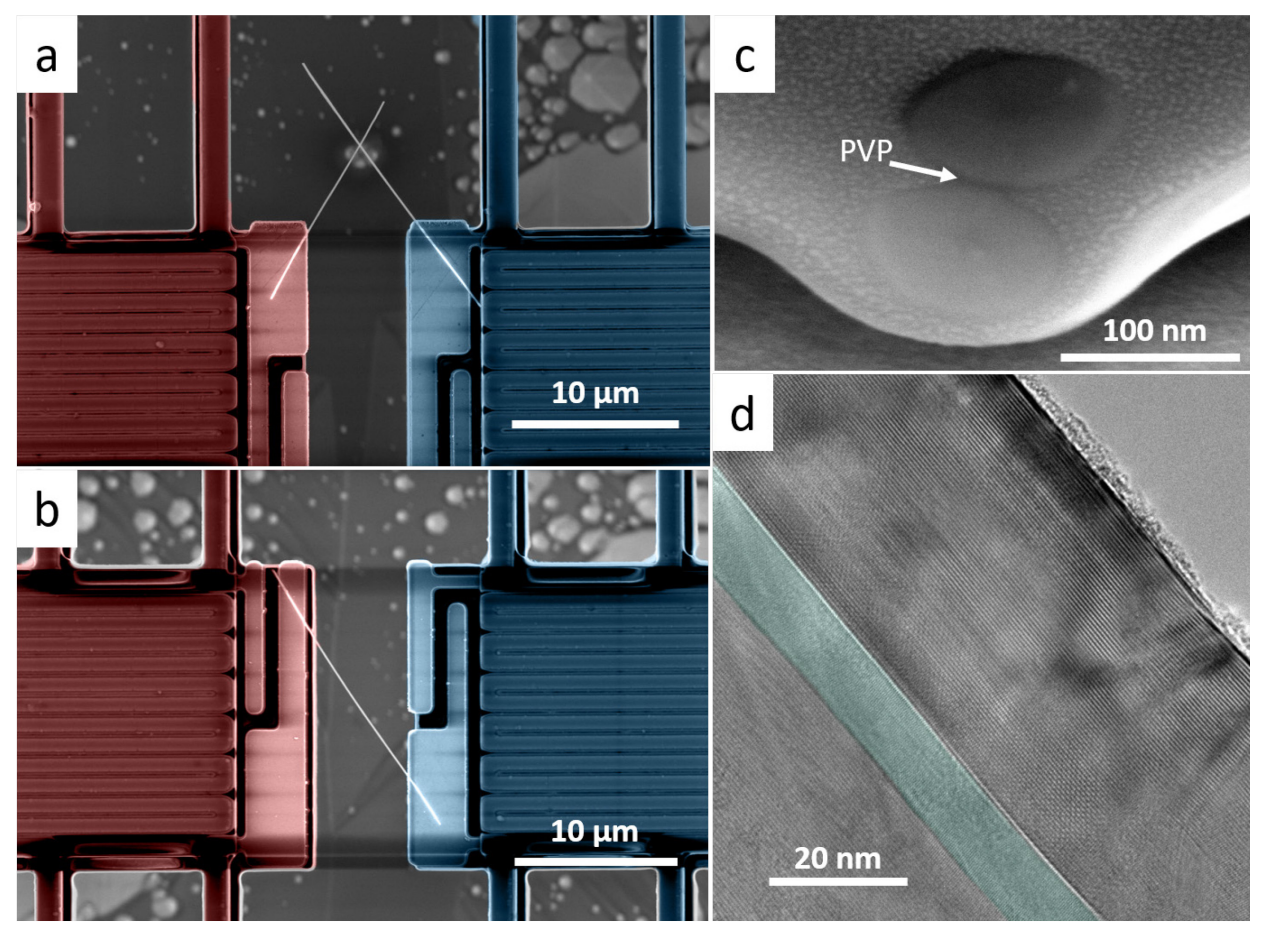


Figure 1. SEM micrographs of (a) a contact sample and (b) a single tube segment on the measurement devices. The diameter of this BNNT is 102 nm and special care has been taken to guarantee the total suspended tube length for heat conduction between the two membranes to be approximately the same. (c) An SEM micrograph showing the cross-section of the contact with a PVP interlayer for the 102 nm diameter BNNTs post the thermal measurement. The image was captured at a tilted angle (52°). (d) A TEM micrograph of the 102 nm diameter BNNT. The tube

layer can be clearly identified and the wall thickness is extracted from the image. The center hollow region is highlighted with green color.

For measurements of the contact thermal resistance with a PVP interlayer between BNNTs, PVP powder (Sigma Aldrich, 437190-25G, molecular weight = 1,300 kg mol⁻¹) was dissolved in ethanol (Sigma Aldrich, 187380-1L) at a ratio of 1:10 (w/w) and drop-cast onto a piece of PDMS. One BNNT segment was picked up with the probe and dipped into the PVP solution for a few seconds. The BNNT was then pulled out of the PVP solution and left in the air for ~20 minutes, which allowed for ethanol to evaporate, resulting in a BNNT with a portion coated with a thin layer of PVP, as identified in the Supporting Information (Section I). This BNNT segment was then aligned with the other bare BNNT segment to form a contact sample with a PVP interlayer between the BNNTs, allowing for the measurement of the BNNT-PVP-BNNT contact.

Table 1 Geometry information of contact samples. D is the outer diameter for the BNNTs. α is the contact angle. A denotes contact area for the contacts. L_s is the suspended length of single continuous tube measurement. L_{cp_tot} and L_{c_tot} are the combined suspended lengths of two segments for the contact samples with and without a PVP interlayer, respectively. t_{wall} and t_{PVP} denote BNNT wall thickness and PVP interlayer thickness, respectively.

Sample ID	D (nm)	t _{wall} (nm)	α (°)	$A (nm^2)$	L _s (μm)	$L_{ m c_tot} \ (\mu m m)$	$L_{ m cp_tot} \ (\mu m m)$	t _{PVP} (nm)
C1	102	43.0	65.5	230.1	11.9	11.7	12.0	13.1
C2	92	37.0	73.0	189.2	10.4	10.2	10.4	13.0
C3	80	32.0	80.1	154.5	9.3	9.3	9.5	12.5
C4	74	31.0	89.0	135.3	11.8	11.6	11.7	13.0
C5	62	25.0	80.0	104.4		10.5	10.3	13.4
C6	67	28.5	97.5	115.8	12.3	12.6		
C7	62	25.0	85.7	109.9	13.4	13.6		
C8	51	20.5	88.2	78.5	9.1	9.2		
С9	47	19.5	77.5	71.5	14.4	14.8		

An SEM micrograph of the contact region between two 102 nm diameter BNNTs is shown in Fig. 1c, where a ~13 nm thick PVP layer between the two BNNTs can be clearly identified. Fig. 1d illustrates a transmission electron microscopy (TEM) micrograph of the layered structure of the same sample. Analysis of the TEM images of all measured BNNTs indicates that the BNNT wall thickness is approximately proportional to the tube diameter, as listed in Table 1.

The measured total thermal resistance of the single continuous tube (R_{tot_S}) and the contact sample (R_{tot_C}) can be written as

$$R_{\text{tot_S}} = R_{\text{C,M}} + R_{\text{w,s}},\tag{1}$$

$$R_{\text{tot C}} = R_{\text{C.M}} + R_{\text{w.c}} + R_{\text{C}}.$$
 (2)

Here, $R_{\text{C,M}}$ is the contact thermal resistance between the sample and the two suspended membranes, while $R_{\text{w,s}}$ and $R_{\text{w,c}}$ represent the intrinsic thermal resistance of the suspended BNNT segment(s) for the single tube and the contact sample, respectively. R_{C} is the contact resistance between the two BNNTs. Significant efforts have been made during sample preparation to guarantee that the length of the suspended BNNTs for heat conduction between the two membranes in the single tube and the contact sample remain approximately the same, with a maximum difference of only 2.5% (see Table 1). Therefore, it is reasonable to assume that $R_{\text{w,s}}$ and $R_{\text{w,c}}$ are approximately the same and can be canceled out in solving for R_{C} through subtracting Eq. 1 from Eq. 2, i.e., $R_{\text{C}} = R_{\text{tot_C}} - R_{\text{tot_S}}$.

Note that for the above derivation to be valid, $R_{C,M}$ needs to remain constant between measurements for the same BNNT sample, which is indeed the case as suggested by the linear profile between the measured resistance and the sample length in Fig. 2b. In addition, the contact

thermal resistance between the BNNT and suspended membranes can be estimated using a fin model;^{23,24} and an analysis indicates that the thermalization distance, i.e., the contact length required for the tube to reach thermal equilibrium with the membranes, is below 2 μ m for all BNNTs. The minimum contact length for all samples is ~2.5 μ m, which further suggests that $R_{\rm C,M}$ should be the same for the continuous wire and contact sample (Section II in the Supporting Information).

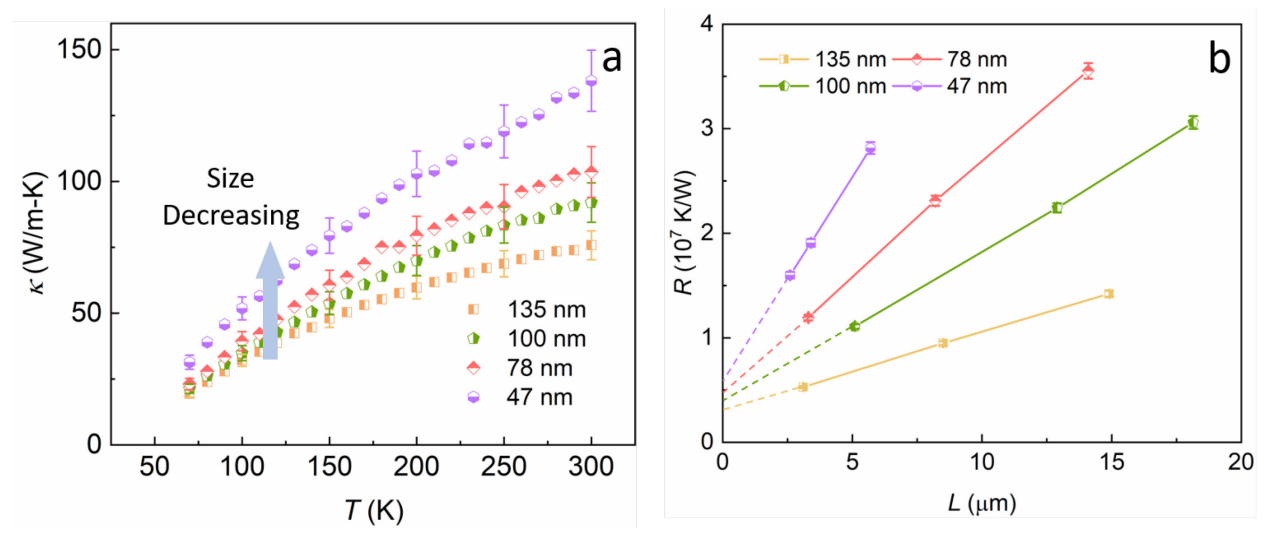


Figure 2. Thermal property of BNNTs. (a) Intrinsic thermal conductivity of different diameter BNNTs. Data were extracted through fitting the resistance-length curves from (b).²³ The extracted intrinsic thermal conductivity increases as the tube size reduces. (b) Thermal resistance *versus* the sample length at 300 K.

Four BNNTs were measured to evaluate the intrinsic thermal conductivity of individual tubes. For each sample, the thermal conductance for three different suspended lengths were measured following an approach used to extract the intrinsic thermal conductivity (κ) of MWCNTs.²³ Fig. 2a indicates that κ increases as the tube diameter reduces, which is a common trend for CNTs and BNNTs as the structural quality is usually better for thinner tubes. Importantly, the linear profile with the suspended length above 3 μ m in Fig. 2b also indicates fully diffusive phonon transport in the tube beyond this length scale. The shortest BNNT segment in the following contact resistance

measurements is $\sim 3.8 \ \mu m$; and therefore, no complication from ballistic phonon transport is involved when comparing $R_{\rm w,s}$ and $R_{\rm w,c}$. In addition, $R_{\rm C,M}$ can be extracted from the measured resistance *versus* length plots (Fig. 2b) as the intercept with the vertical axis, and the weight of $R_{\rm C,M}$ is always less than 15%.

Next, $R_{\rm C}$ between bare BNNTs was measured for eight samples of different diameters, as listed in Table 1. The tube length, diameter and PVP layer thickness were obtained from SEM examination while the tube wall thickness was extracted *via* TEM studies. Fig. 3a shows extracted $R_{\rm tot_C}$, $R_{\rm tot_S}$, and $R_{\rm C}$ for a 74 nm sample. At room temperature, $R_{\rm C}$ contributes ~35% to $R_{\rm tot_C}$, well beyond the measurement uncertainty (Section III in the Supporting Information).

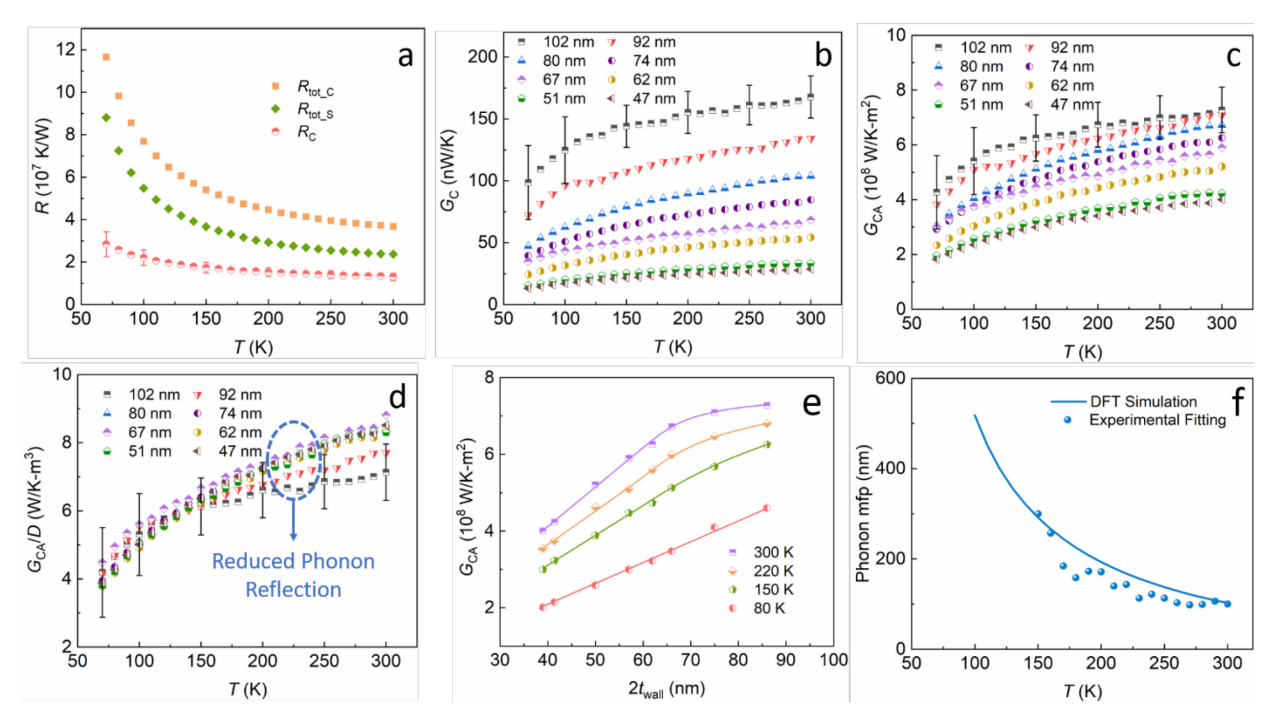


Figure 3. Contact thermal resistance between bare BNNTs. (a) Thermal resistance components of a 74 nm diameter sample. (b) Interfacial thermal conductance, $G_{\rm C}$, for BNNT-BNNT contact. $G_{\rm C}$ shows a clear size dependence. (c) Interfacial thermal conductance per unit area, $G_{\rm CA}$, for BNNT-BNNT contact. $G_{\rm CA}$ still increases as size increases. (d) $G_{\rm CA}$ normalized by D. Data for the 92 nm and 102 nm diameter samples deviate from the others at elevated temperatures above 150 K. (e) $G_{\rm CA}$ versus the doubled wall thickness. While $G_{\rm CA}$ increases linearly with the wall thickness in the

low temperature regime, the increasing trend gets flatter as the wall thickness increase beyond 150 K. (f) Extracted cross-plane phonon mfp from fitting the experimental data and DFT simulations.

Fig. 3b plots the extracted contact thermal conductance, $G_{\mathbb{C}}$, which increases monotonically with the tube diameter. To further understand the phonon transport mechanism at the tube-tube contact, we solve for contact thermal conductance per unit area, G_{CA} . To do so, we calculated the contact area using the Maugis model, 19,25 as listed in Table 1. As shown in Fig. 3c, G_{CA} , which is normally size-independent, still increases with the tube diameter, indicating more interesting transport physics at the contact. Similar phenomenon has been observed for MWCNTs, 19 which is explained based on three coupled mechanisms. First, the phonon mean free path (mfp) along the radial direction of the tube in MWCNTs is ~200 nm, well-beyond the traditionally believed value. This renders ballistic transport of phonons through the contact that can be reflected by the innermost layer of the receiving tube back into the emitting tube, which do not contribute to thermal transport from one tube to the other. Only when phonons experience scattering in the receiving tube, they deliver energy across the contact and contribute to the contact thermal conductance. Since the possibility of phonons getting thermalized when they travel in the receiving tube is proportional to the wall thickness, and hence the tube diameter, G_{CA} becomes a function of diameter. Note that for the above picture to be valid, phonons responsible for the contact thermal conductance need to transport largely along the tube radial direction, which is indeed the case considering the phonon focusing effect induced by the drastically different bonding strengths within each tube layer and between different tube layers.

Similar physical picture can be applied to contacts between BNNTs and to verify this, G_{CA}/D , where D is the tube diameter, is plotted in Fig. 3d. It can be seen that the G_{CA}/D curves for different diameter samples overlap with each other, except for the 92 nm and 102 nm samples at elevated

temperatures. At room temperature, G_{CA}/D for the 102 nm sample is 16% lower than the average value for the six thinner samples, which is well beyond the measurement uncertainty. This deviation can be explained by the fact that as temperature increases, the phonon mfp gets shorter and becomes comparable to $2t_{wall}$, where t_{wall} is the wall thickness.

It has been shown that the phonon mfp along the c-axis for graphite and MoS₂ could be well over 100 nm;²⁶⁻²⁸ however, no such data have been reported for boron nitride. As such, we estimate the phonon mfp for boron nitride based on the diameter dependence of G_{CA} . Fig. 3e plots G_{CA} as a function of the doubled wall thickness ($2t_{wall}$) at different temperatures, and the linear trend can be clearly observed at 80 K. Above 150 K, the increasing trend of G_{CA} becomes flatter as $2t_{wall}$ increases beyond ~66 nm, indicating that the phonon mfp above 150 K along the c-axis of boron nitride should be comparable to this value.

A model can be constructed based on this observation to extract the phonon mfp. The probability of a phonon traveling over a distance ΔL along the radial direction without being scattered can be written as $P = e^{-\frac{\Delta L}{\lambda}}$, ²⁹ where λ is the phonon mfp. Considering that phonons will be reflected at the innermost layer and travel through the tube wall twice, the energy absorbed (E_a) by the receiving tube can be related to the incoming energy (E_i) carried by phonons from the other tube as

$$E_a = (1 - e^{-\frac{2t_{wall}}{\lambda}})E_i. \tag{3}$$

The effective phonon transmission probability across the contact, α , as a result of phonon reflection at the innermost layer, can then be written as

$$\alpha = \frac{E_a}{E_i} = 1 - e^{-\frac{2t_{wall}}{\lambda}}.$$
 (4)

Note that since λ depends on temperature so α is also a function of temperature. This leads to the following relation

$$G_{CA}(T) = (1 - e^{-\frac{2t_{wall}}{\lambda}})G_{CA,0},$$
 (5)

where $G_{CA,\theta}$ is the contact thermal conductance per unit area without the effect of phonon reflection. λ and $G_{CA,\theta}$ can be extracted from fitting the experimental data set of G_{CA} versus $2t_{wall}$. The resulting phonon mfp is shown in Fig. 3f. At 300 K, λ is ~100 nm while at 150 K, λ increases to 300 nm. This observation is consistent with the findings that the phonon mfp along the c-axis of graphite and MoS₂ is on the order of 100 nm, much longer than the traditionally believed value of just a few nanometers. 30,31

To further verify this result, density functional theory (DFT) based calculations were performed, which was based on the Vienna *ab initio* simulation package (VASP).³² An energy cutoff of 520 eV was chosen for the plane wave basis sets in the projector augmented wave (PAW) method.³³ The exchange correlation interaction was treated with the general gradient approximation (GGA) in the Perdew–Burke–Ernzerhof (PBE) parametrization considering the vdW correction.^{34,35} The phonon mfp was obtained by solving the phonon Boltzmann transport equation (BTE) under the relaxation time approximation as implemented in the Sheng BTE code.³⁶ As shown in Fig. 3f, the simulation fits the extracted phonon mfp from the experimental data reasonably well. The slightly lower values derived from the experimental data could be due to imperfections involved in the sample quality such as defects in the tubes and the surface residues at the contact.

To explore the effect of a thin polymer interlayer on the contact thermal resistance, five samples with a BNNT-PVP-BNNT contact morphology have been measured. The thickness of the PVP layer between two BNNTs is ~13 nm for all five samples, as listed in Table 1. Fig. 4a shows the extracted $R_{\rm C}$ for the 74 nm tube with and without the thin PVP layer. Interestingly, contrary to the expectation that the PVP layer will add additional resistance and increase $R_{\rm C}$, it actually leads to a lower $R_{\rm C}$. It is worth noting that the reduction percentage increases as temperature drops. More interestingly, results in Fig. 4b suggest that the contact resistance change $\Delta R_{\rm C}$ ($\Delta R_{\rm C} = R_{\rm C,PVP} - R_{\rm C,Bare}$, where $R_{C,PVP}$ and $R_{C,Bare}$ are contact thermal resistance with and without the PVP layer, respectively) is positive for larger tubes and negative for smaller tubes, which means that the PVP interlayer increases $R_{\rm C}$ for the 80, 92, 102 nm diameter tubes but reduces the corresponding value for the 62 and 74 nm diameter tubes. This observation illustrates a bi-directional modulation of $G_{\rm C}$ by the PVP interlayer. In fact, with the PVP interlayer, $G_{\rm C}$ presents an opposite size dependence compared to the case for bare tubes (Fig. 4c); and for the 102 nm diameter sample, after introducing a PVP interlayer, G_C is greatly reduced, while for the 74 nm diameter sample, G_C is enhanced (Fig. 4d).

The bi-directional modulation of the contact thermal resistance indicates competing effects of the PVP interlayer on $R_{\rm C}$. On one hand, the PVP interlayer introduces additional thermal resistance as it is of very low thermal conductivity (\sim 0.23 W/m-K at 300 K); on the other hand, the effective contact area between the BNNTs is enlarged significantly by the PVP interlayer. While it seems that these two competing mechanisms could be responsible for the opposite trends of the thermal resistance for the contacts between BNNTs of large and small diameters, in-depth analysis discloses more interesting physical picture behind the observation.

First, the enhancement of the contact thermal resistance for larger diameter tubes cannot be simply regarded as the additional thermal resistance of the PVP. For the 80 nm diameter tube, for example, ΔR_C at 300 K is only 3.4×10⁶ K/W. If this resistance change is treated as that of the PVP layer, it can be calculated as $\Delta R_C = t_{PVP}/\kappa_{PVP}A_C$, where t_{PVP} and κ_{PVP} are the thickness and thermal conductivity of the PVP layer, respectively, and A_C is the contact area. Taking t_{PVP} as 12.5 nm and κ_{PVP} as 0.23 W/m-K, the resulting A_C is 16,105 nm², which corresponds a characteristic size of 143.2 nm if the contact is assumed to be a circle. This dimension is beyond the tube diameter so treating ΔR_C as the additional resistance from the PVP interlayer is not reasonable.

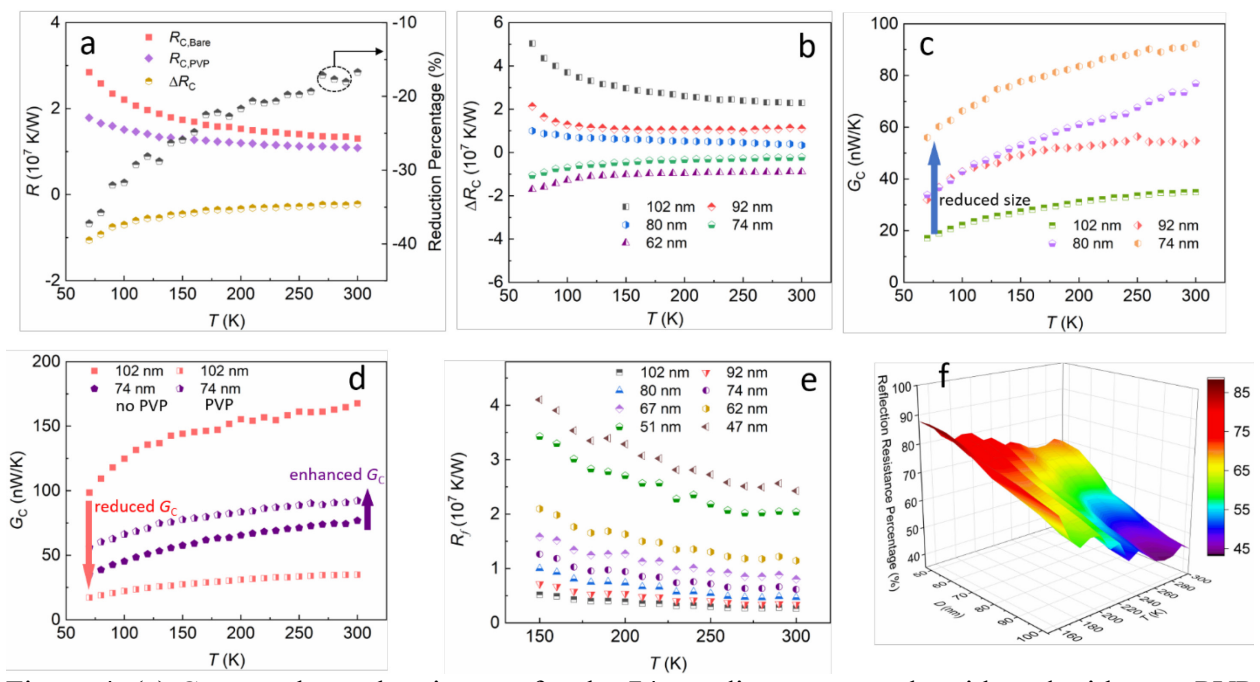


Figure 4. (a) Contact thermal resistance for the 74 nm diameter sample with and without a PVP layer (Left axis), and the percentage reduction with the PVP layer is also shown (Right axis). $\Delta R_{\rm C}$ is the contact thermal resistance difference with and without PVP layer. Surprisingly, $R_{\rm C}$ becomes smaller with the PVP interlayer. (b) $\Delta R_{\rm C}$ for samples of different sizes. (c) $G_{\rm C}$ with the PVP layer as a function of the tube size. Counter-intuitively, as size reduces, $G_{\rm C}$ increases, opposite to the trend for bare tube contacts. (d) Bi-directional modulation of $G_{\rm C}$ by the PVP layer. With the PVP interlayer, $G_{\rm C}$ decreases for the 102 nm diameter sample and increases for the 74 nm diameter sample. (e) Contact thermal resistance induced by phonon reflection, R_f , for contacts between bare tubes. R_f increases rapidly as the tube size reduces. (f) Contribution of R_f to $R_{\rm C}$. The percentage contribution from R_f increases as the temperature and tube diameter reduce.

In fact, the PVP interlayer fundamentally altered the phonon transport picture at the contact. For contacts between bare BNNTs, phonons from the emitting tube can ballistically transmit through the contact and G_{CA} is largely determined by whether these phonons can be thermalized in the receiving tube; or equivalently, to what extent these phonons are reflected back into the emitting tube determines $R_{\rm C}$. However, the PVP interlayer disrupts this ballistic transport mechanism as phonons can only diffuse through the PVP layer. In fact, it has been shown that a monolayer of organic residue between two boron nanoribbons can completely eliminate the ballistic transmission of phonons through the van der Waals interface between the two ribbons.³⁷ In this case, the PVP interlayer largely determines the contact thermal resistance. This is the case for the larger tubes when phonon reflection is not the dominant factor at the contact due to large t_{wall} . As shown in Fig. 4d, for the 102 nm diameter sample, $G_{\text{C,Bare}}$ is much larger than $G_{\text{C,PVP}}$. The reduction is primarily caused by the resistance of the PVP layer. However, as tube size reduces, phonon reflection contributes more to $R_{C,Bare}$. As shown in Fig. 4e, phonon reflection induced thermal resistance R_f ($R_f = R_{C,Bare} - 1/AG_{CA,0}$, where A is the contact area between bare tubes and $G_{CA,0}$ is the thermal conductance per unit area without phonon reflection from the fitting) increases dramatically as the tube size reduces. Fig. 4f plots contribution of R_f to total resistance versus the tube diameter and temperature, which indicates that phonon reflection contributes ~44% to R_C for the 102 nm sample and increases to \sim 71% for the 47 nm diameter sample at room temperature. At low temperatures, R_f contributes even more.

As discussed above, the additional PVP layer can eliminate the ballistic transmission of phonons thus remove R_f from R_C at the cost of introducing interfacial resistance ($R_{\text{Interface}}$) and polymer resistance (R_{PVP}). The net effect, ΔR_C , follows $\Delta R_C = R_{\text{PVP}} + R_{\text{interface}} - R_f$. For larger

tubes, R_f is small compared to $R_{\text{PVP}} + R_{\text{interface}}$, hence ΔR_{C} is positive. As size reduces, R_f increases, and ΔR_{C} reduces and eventually becomes negative. This can also explain the temperature dependence of the relative resistance reduction in Fig. 4a. At low temperatures, phonon mfp increases, leading to a much larger R_f while resistance posed by PVP doesn't increase as much. Thus, reduction is more profound.

In polymer composites, direct filler-filler contacts have usually been considered beneficial for thermal transport by reducing $R_{\rm C}$ and forming a percolated filler thermal pathway. ^{18,38-40} However, for highly anisotropic materials like CNTs and BNNTs, as a result of phonon reflection, $R_{\rm C}$ between tubes could be comparable to interfacial resistance (1-2×10⁻⁹ m² K/W for BN based composites) ^{41,42} and be equivalent to the resistance of a polymer layer of a few tens of nanometers thick, which could render more than one order of magnitude reduction in thermal conductivity for CNT network. ^{19,43-46} In this case, a thin polymer layer between CNTs or BNNTs could actually reduce the contact thermal resistance and result in a more thermally conductive filler thermal pathway. This is especially true for BNNT-based composites, as $R_{\rm interface}$ between BNNTs and polymer matrices is believed to be smaller than that between CNTs and polymers. ⁴⁷⁻⁵⁰

In summary, this study discloses interesting observation of contact thermal resistance between bare BNNTs and the bi-directional modulation of the contact resistance from a PVP interlayer. Analysis indicates that these results are due to conversion from ballistic phonon transmission and back reflection for contacts between bare BNNTs to diffusive transport through a PVP interlayer. These previously unrecognized phenomena and understandings provide important insights into better tuning the thermal properties of BNNT-polymer composites for different applications.

Methods

Thermal transport property measurements: The thermal resistance measurements of BNNT

samples were conducted in a cryostat ((Janis CCS-400/204) under a high vacuum ($<1\times10^{-6}$ mbar).

Dual radiation shields were used to minimize the effects of radiation on the heat conduction

measurements. The measurements were conducted following a well-established procedure²¹⁻²³ that

has been employed to measure various nanowires and nanotubes. A Wheatstone bridge setup was

adopted at the sensing side of the device to improve measurement sensitivity,²² which allows for

a measurement resolution of ~0.1 nW/K at room temperature based on the selected settings for

measurements in this study.

MICROSCOPY. SEM examination is conducted with either a Zeiss Merlin SEM with the

GEMINI II column or the integrated SEM in a dual beam FEI Helios NanoLab G3 CX FIB-SEM.

TEM studies are done using an FEI Tecnai G2 Osiris S/TEM. The cross-section of the contact is

obtained through first depositing a Pt/C coating using electron beam induced deposition and then

cutting at different locations with the focused ion beam, following a procedure as detailed in

previous report. 51,52

ASSOCIATED CONTENT

Supporting Information

The Supporting Information is available free of charge on the ACS Publications website.

AUTHOR INFORMATION

Corresponding Author

*E-mail: deyu.li@vanderbilt.edu.

Author Contributions

15

Z.P., M.L.F. and Y.Z. prepared PVP coated samples. Z.P. performed the thermal measurements. Y.T. conducted DFT simulations. Z.P. and D.L. analyzed data and wrote the manuscript. Z.P. and J.M. conducted the TEM examination. Z.L. and D.L. supervised the project. All authors discussed the results and commented on the manuscript.

Notes

The authors declare no competing financial interest.

ACKNOWLEDGMENTS

The authors thank the financial support from the U.S. National Science foundation (Award#1903645 and #1532107). M.L.F. acknowledges the graduate fellowship support from the National Aeronautics and Space Administration (NSTRF18_80NSSC18K1165). Y.T. acknowledges financial support from the China Scholarship Council (CSC#201806090027). This work was performed in part at the Cornell NanoScale Facility, an NNCI member supported by NSF Grant NNCI-2025233.

References

- (1) Pop, E. Energy dissipation and transport in nanoscale devices. *Nano Res.* **2010**, *3*(3), 147-169.
- (2) Moore, A. L.; Shi, L. Emerging challenges and materials for thermal management of electronics. *Mater. Today* **2014**, *17*(4), 163-174.
- (3) Xu, X.; Chen, J.; Zhou, J.; Li, B. Thermal conductivity of polymers and their nanocomposites. *Adv. Mater.* **2018**, *30*(17), 1705544.
- (4) Guthy, C.; Du, F.; Brand, S.; Winey, K.I.; Fischer, J.E. Thermal Conductivity of Single-Walled Carbon Nanotube/PMMA Nanocomposites. *J. Heat Transfer* **2009**, *129*(8), 1096-1099.
- (5) King, J.A.; Gaxiola, L.D.; Johnson, B.A., Keith, J.M. Thermal conductivity of carbon-filled polypropylene-based resins. *J. Compos. Mater.* **2010**, *44*(7), 839-855.
- (6) Song, Y.S.; Youn, J.R. Influence of dispersion states of carbon nanotubes on physical properties of epoxy nanocomposites. *Carbon* **2005**, *43*(7), 1378-1385.
- (7) Zhou, T.; Wang, X.; Gu, M.; Liu, X. Study of the thermal conduction mechanism of nano-SiC/DGEBA/EMI-2,4 composites. *Polymer* **2008**, *49*(21), 4666-4672
- (8) Yu, S.; Hing, P.; Hu, X. Thermal conductivity of polystyrene–aluminum nitride composite. *Composites A* **2002**, *33* (2), 289-292.

- (9) Gu, J.; Zhang, Q.; Dang, J.; Zhang, J.; Yang, Z. Thermal conductivity and mechanical properties of aluminum nitride filled linear low-density polyethylene composites. *Polym. Eng. Sci.* **2009**, *49*(5), 1030-1034.
- (10) Xu, J.; Munari, A.; Dalton, E.; Mathewson, A.; Razeeb, K.M. Silver Nanowire Array-Polymer Composite as Thermal Interface Material. *J. Appl. Phys.* **2009**, *106*, 124310.
- (11) Wang, S.; Cheng, Y.; Wang, R.; Sun, J.; Gao, L. Highly Thermal Conductive Copper Nanowire Composites with Ultralow Loading: Toward Applications as Thermal Interface Materials. *ACS Appl. Mater. Interfaces* **2014**, *6*(9), 6481–6486.
- (12) Boudenne, A.; Ibos, L.; Fois, M.; Majeste, J.C.; Gehin, E. Electrical and thermal behavior of polypropylene filled with copper particles. *Composites A* **2005**, *36*(11), 1545-1554.
- (13) Balachander, N.; Seshadri, I.; Mehta, R.J.; Schadler, L.S.; Borca-Tasciuc, T.; Keblinski, P.; Ramanath, G. Nanowire-Filled Polymer Composites with Ultrahigh Thermal Conductivity. *Appl. Phys. Lett.* **2013**, *102*, 093117.
- (14) Zhi, C.; Bando, Y.; Terao, T.; Tang, C.; Kuwahara, H.; Golberg, D. Towards thermoconductive, electrically insulating polymeric composites with boron nitride nanotubes as fillers. *Adv. Funct. Mater.* **2009**, *19*(12), 1857-1862.
- (15) Terao, T.; Bando, Y.; Mitome, M.; Zhi, C.; Tang, C.; Golberg, D. Thermal conductivity improvement of polymer films by catechin-modified boron nitride nanotubes. *J. Phys. Chem. C* **2009**, *113*(31), 13605-13609.
- (16) Yang, X.; Guo, Y.; Han, Y.; Li, Y.; Ma, T.; Chen, M.; Kong, J.; Zhu, J.; Gu, J. Significant improvement of thermal conductivities for BNNS/PVA composite films via electrospinning followed by hot-pressing technology. *Compos. B. Eng.* **2019**, *175*, 107070.
- (17) Chen, H.; Ginzburg, V.V.; Yang, J.; Yang, Y.; Liu, W.; Huang, Y.; Du, L.; Chen, B. Thermal conductivity of polymer-based composites: Fundamentals and applications. *Prog. Polym. Sci.* **2016**, *59*, 41-85.
- (18) Han, Z.; Fina, A. Thermal conductivity of carbon nanotubes and their polymer nanocomposites: A review. *Prog. Polym. Sci.* **2011**, *36*(7), 914-944.
- (19) Yang, J.; Shen, M.; Yang, Y.; Evans, W.J.; Wei, Z.; Chen, W.; Zinn, A.A.; Chen, Y.; Prasher, R.; Xu, T.T.; Keblinski, P.; Li, D. Phonon transport through point contacts between graphitic nanomaterials. *Phys. Rev. Lett.* **2014**, *112*(20), 205901.
- (20) Shi, L.; Li, D.; Yu, C.; Jang, W.; Kim, D.; Yao, Z.; Kim, P.; Majumdar, A. Measuring Thermal and Thermoelectric Properties of One-Dimensional Nanostructures Using a Microfabricated Device. *J. Heat Transfer* **2003**, *125*(5), 881–888.
- (21) Wingert, M.C.; Chen, Z. C. Y.; Kwon, S.; Xiang, J.; Chen, R. Ultra-Sensitive Thermal Conductance Measurement of One-Dimensional Nanostructures Enhanced by Differential Bridge. *Rev. Sci. Instrum.* **2012**, *83*(2), 024901.
- (22) Yang, L.; Yang, Y.; Zhang, Q.; Zhang, Y.; Jiang, Y.; Guan, Z.; Gerboth, M.; Yang, J.; Chen, Y.; Walker, D.G.; Xu, T.T.; Li, D. Thermal conductivity of individual silicon nanoribbons. *Nanoscale*, **2016**, *8*(41), 17895-17901.
- (23) Yang, J.; Yang, Y.; Waltermire, S.W.; Gutu, T.; Zinn, A.A.; Xu, T.T.; Chen, Y.; Li, D. Measurement of the intrinsic thermal conductivity of a multiwalled carbon nanotube and its contact thermal resistance with the substrate. *Small* **2011**, 7(16), 2334-2340.
- (24) Yu, C; Saha, S.; Zhou, J.; Shi, L.; Cassell, A.M.; Cruden, B.A.; Ngo, Q.; Li, J. Thermal contact resistance and thermal conductivity of a carbon nanofiber. *J. Heat Transfer* **2006**, *128*(3), 234-239.

- (25) Maugis, D. Adhesion of spheres: the JKR-DMT transition using a Dugdale model. *J. Colloid Interface Sci.* **1992**, *150*(1), 243-269.
- (26) Zhang, H.; Chen, X.; Jho, Y.D.; Minnich, A.J. Temperature-dependent mean free path spectra of thermal phonons along the c-axis of graphite. *Nano letters* **2016**, *16*(3), 1643-1649.
- (27) Fu, Q.; Yang, J.; Chen, Y.; Li, D.; Xu, D. Experimental evidence of very long intrinsic phonon mean free path along the c-axis of graphite. *Appl. Phys. Lett.* **2015**, *106*(3), 031905.
- (28) Sood, A.; Xiong, F.; Chen, S.; Cheaito, R.; Lian, F.; Asheghi, M.; Cui, Y.; Donadio, D.; Goodson, K.E.; Pop, E. Quasi-ballistic thermal transport across MoS₂ thin films. *Nano letters* **2019**, 19(4), 2434-2442.
- (29) Liang, Z.; Sasikumar, K.; Keblinski, P. Thermal transport across a substrate-thin-film interface: effects of film thickness and surface roughness. *Phys. Rev. Lett.* **2014**, *113*(6), 065901.
- (30) Shen, M.; Schelling, P. K.; Keblinski, P. Heat transfer mechanism across few-layer graphene by molecular dynamics. *Phys. Rev. B*, **2013**, 88(4), 045444.
- (31) Tanaka, T.; Suzuki, H. The thermal diffusivity of pyrolytic graphite at high temperatures. *Carbon* **1972**, *10*(3), 253-257.
- (32) Kresse, G.; Furthmüller, J. Efficiency of ab-initio total energy calculations for metals and semiconductors using a plane-wave basis set. *Comput. Mater. Sci.* **1996**, *6*(1), 15-50.
- (33) Kresse, G.; Joubert, D. From ultrasoft pseudopotentials to the projector augmented-wave method. *Phys. Rev. B.* **1999**, *59*(3), 1758-1775.
- (34) Perdew, J.P.; Burke, K.; Ernzerhof, M. Generalized gradient approximation made simple. *Phys. Rev. Lett.* **1996**, 77(18), 3865-3868.
- (35) Grimme, S.; Antony, J.; Ehrlich, S.; Krieg, H. A consistent and accurate ab initio parametrization of density functional dispersion correction (DFT-D) for the 94 elements H-Pu. *J. Chem. Phys.* **2010**, *132*(15), 154104.
- (36) Li, W.; Carrete, J.; Katcho, N.A.; Mingo, N. ShengBTE: A solver of the Boltzmann transport equation for phonons. *Comput. Phys. Commun.* **2014**, *185*(6), 1747-1758.
- (37) Yang, J.; Yang, Y.; Waltermire, S.W.; Wu, X.; Zhang, H.; Gutu, T.; Jiang, Y.; Chen, Y.; Zinn, A.A.; Prasher, R.; Xu, T.T.; Li, D. Enhanced and switchable nanoscale thermal conduction due to van der Waals interfaces. *Nat. Nanotechnol.* **2012**, *7*(2), 91-95.
- (38) Pashayi, K.; Fard, H.R.; Lai, F.; Iruvanti, S.; Plawsky, J.; Borca-Tasciuc, T. High thermal conductivity epoxy-silver composites based on self-constructed nanostructured metallic networks. *J. Appl. Phys.* **2012**, *111*(10), 104310.
- (39) Yorifuji, D.; Ando, S. Enhanced thermal conductivity over percolation threshold in polyimide blend films containing ZnO nano-pyramidal particles: advantage of vertical double percolation structure. *J. Mater. Chem.* **2011**, *21*(12), 4402-4407.
- (40) Xu, J.; Munari, A.; Dalton, E.; Mathewson, A.; Razeeb, K.M. Silver nanowire array-polymer composite as thermal interface material. *J. Appl. Phys.* **2009**, *106*(12), 124310.
- (41) Wang, Z.; Chen, M.; Liu, Y.; Duan, H.; Xu, L.; Zhou, L.; Xu, J.; Lei, J.; Li, Z. Nacre-like composite films with high thermal conductivity, flexibility, and solvent stability for thermal management applications. *J. Mater. Chem. C* **2019**, 7(29), 9018-9024.
- (42) Fu, C.; Li, Q.; Lu, J.; Mateti, S.; Cai, Q.; Zeng, X.; Du, G.; Sun, R.; Chen, Y.; Xu, J.; Wong, C.P. Improving thermal conductivity of polymer composites by reducing interfacial thermal resistance between boron nitride nanotubes. *Compos Sci Technol.* **2018**, *165*, 322-330.
- (43) Zhong, H.; Lukes, J.R. Interfacial thermal resistance between carbon nanotubes: molecular dynamics simulations and analytical thermal modeling. *Phys. Rev. B* **2006**, *74*(12), 125403.

- (44) Foygel, M.; Morris, R.D.; Anez, D.; French, S.; Sobolev, V.L. Theoretical and computational studies of carbon nanotube composites and suspensions: Electrical and thermal conductivity. *Phys. Rev. B*, **2005**, *71*(10), 104201.
- (45) Bonnet, P.; Sireude, D.; Garnier, B.; Chauvet, O. Thermal properties and percolation in carbon nanotube-polymer composites. *Appl. Phys. Lett.* **2007**, *91*(20), 201910.
- (46) Wu, H.; Drzal, L.T. High thermally conductive graphite nanoplatelet/polyetherimide composite by precoating: Effect of percolation and particle size. *Polym. Compos.***2013**, *34*(12), 2148-2153.
- (47) Zhi, C.; Zhang, L.; Bando, Y.; Terao, T.; Tang, C.; Kuwahara, H.; Golberg, D. New crystalline phase induced by boron nitride nanotubes in polyaniline. *J. Phys. Chem. C* **2008**, *112*(45), 17592-17595.
- (48) Zhi, C.; Bando, Y.; Tang, C.; Honda, S.; Sato, K.; Kuwahara, H.; Golberg, D. Characteristics of boron nitride nanotube–polyaniline composites. *Angew. Chem.* **2005**, *117*(48), 8143-8146.
- (49) Velayudham, S.; Lee, C.H.; Xie, M.; Blair, D.; Bauman, N.; Yap, Y.K.; Green, S.A.; Liu, H. Noncovalent Functionalization of Boron Nitride Nanotubes with Poly (p-phenylene-ethynylene) s and Polythiophene. *ACS Appl. Mater. Interfaces* **2010**, *2*(1), 104-110.
- (50) Meng, W.; Huang, Y.; Fu, Y.; Wang, Z.; Zhi, C. Polymer composites of boron nitride nanotubes and nanosheets. *J. Mater. Chem. C* **2014**, *2*(47), 10049-10061.
- (51) Zhang, Q.; Liu, C.; Liu, X.; Liu, J.; Cui, Z.; Zhang, Y.; Zhang, Y.; Yang, L.; Zhao, Y. Xu, T.T.; Chen, Y.; Wei, J.; Mao, Z.; Li, D. Thermal transport in quasi-1D van der Waals crystal Ta2Pd3Se8 nanowires: size and length dependence. *ACS Nano* **2018**, *12*(3), 2634-2642.
- (52) Zhao, Y.; Fitzgerald, M. L.; Tao, Y.; Pan, Z.; Sauti, G.; Xu, D.; Xu, Y.; Li, D. Electrical and thermal transport through silver nanowires and their contacts: Effects of elastic stiffening. *Nano Letters* **2020**, *20* (10), 7389-7396.

Table of Contents Graphic

